

Learning Global and Local Consistent Representations for Unsupervised Image Retrieval via Deep Graph Diffusion Networks

Zhiyong Dou, Haotian Cui, and Bo Wang, *Member, IEEE*,

Abstract—Diffusion has shown great success in improving accuracy of unsupervised image retrieval systems by utilizing high-order structures of image manifold. However, existing diffusion methods suffer from three major limitations: 1) they usually rely on local structures without considering global manifold information; 2) they focus on improving pair-wise similarities within existing images input output *transductively* while lacking flexibility to learn representations for novel unseen instances *inductively*; 3) they fail to scale to large datasets due to prohibitive memory consumption and computational burden due to intrinsic high-order operations on the whole graph. In this paper, to address these limitations, we propose a novel method, **Graph Diffusion Networks** (GRAD-Net), that adopts graph neural networks (GNNs), a novel variant of deep learning algorithms on irregular graphs. GRAD-Net learns semantic representations by exploiting both local and global structures of image manifold in an unsupervised fashion. By utilizing sparse coding techniques, GRAD-Net not only preserves global information on the image manifold, but also enables scalable training and efficient querying. Experiments on several large benchmark datasets demonstrate effectiveness of our method over state-of-the-art diffusion algorithms for unsupervised image retrieval.

Index Terms—Unsupervised Image Retrieval, Graph Diffusion Networks, Sparse Coding.

1 INTRODUCTION

UNSUPERVISED image retrieval refers to the task of obtaining relevant instances in a database to a given query without any labeled information, forming an important basis for various applications like information search and database management [1], [2]. Traditionally, this is accomplished by computing either a predefined pairwise similarity (e.g., Euclidean distances) or improved high-order similarities by adopting random-walk style process (e.g., diffusion [3]). It is widely known that, no single metric can generate reliable retrieval performances thanks to the “curse” of dimensionality [4]. For this reason, much of the research on unsupervised image retrieval has focused on exploiting diffusion process to learn context-sensitive affinity measures [5], [6].

The same principle to capture the manifold geometry applies to most existing diffusion methods. First, the manifold is interpreted as a weighted graph, where each instance is represented as a node, and edges connect these nodes with weights derived from the pairwise similarity values. The pairwise affinities are then updated iteratively by diffusing along the graph geometry. This diffusion process, originally provided in [7], typically follows the concept of random

walk, where a transition matrix determines probabilities of transiting from one node to another, whose values are proportional to the affinities between those nodes. Eventually, the updated affinity values in turn improve the retrieval results. To illustrate the concept, let us consider the following toy example. As shown in Fig. 1, each point here is a simple analogy to the feature vector of an image. The data distribution consists of four letters, each having 1500 points. The queries are displayed as the star nodes. An ideal result for this retrieval example is that the points in the same letter as the query should be ranked prior than those in the other letters. Clearly, Euclidean distance as an similarity metric (See Fig. 1a) is inadequate for this task, while in comparison, after diffusing the similarities though the geometry and capturing the manifold structure, the retrieval result is significantly improved (See Fig. 1b).

Recently, the success of deep neural networks provides powerful interfaces for image features with rich semantic information. Models, particularly deep convolutional networks [8]–[11], pre-trained on large datasets such as ImageNet [12] and Landmarks [8] are increasingly being used for feature extraction. Diffusion is then deployed on these features to further improve the retrieval result.

However, these diffusion-based methods suffer from three main limitations. First, they usually rely on local structures without considering global manifold information. That is, sparsified graphs based on neighborhood are extensively used without considering the *cluster* structures as a whole. Second, they focus on improving pair-wise similarities within existing images *transductively* while lacking the flexibility to learn representations for unseen instances *inductively*. In other words, it is difficult to generalize the diffusion models to novel databases without re-training the

- Z. Dou is with Peter Munk Cardiac Center, Toronto, ON M5G 2N2, and the University of Toronto, Toronto, Ontario M5S 1A1, Canada. He is also with the School of Electronic Information and Communications, Huazhong University of Science and Technology, Wuhan, Hubei 430074, China.
E-mail: zydou@hust.edu.cn
- H. Cui and B. Wang are with Vector Institute, Toronto, ON M5G 1M1 and University of Toronto, Toronto, Ontario M5S 1A1, Canada. B. Wang is also with Peter Munk Cardiac Center.
E-mail: htcui@cs.toronto.edu, bowang@vectorinstitute.ai

Zhiyong Dou and Haotian Cui contribute equally. Corresponding author: Bo Wang

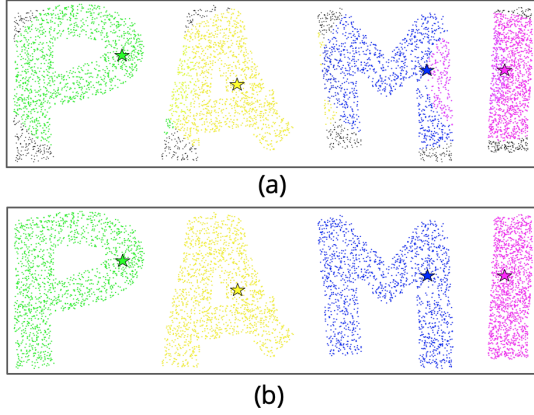


Fig. 1. Diffusion on a synthetic toy dataset. Four queries are marked as stars. (a) retrieval results based on euclidean distance; (b) retrieval results after diffusion.

models. Last, they usually fail to scale up to large datasets due to prohibitive memory consumption and computational burden resulted from intrinsic high-order operations on the whole graphs.

Graph neural networks (GNNs) [13]–[16], have recently emerged as a promising line of research that adopts convolutional operators on irregular inputs like graphs. For instance, there has been an increasing interest on applying GNNs to citation network analysis [13], [17], collaborative filtering [18] and knowledge graphs [19], that achieved state-of-the-art performances. However, most existing GNNs rely on supervised information to train an effective model. This prevents direct adoption of GNNs on the aforementioned image retrieval tasks of interest due to a lack of labeled data.

In this paper, we propose a novel approach, *Graph Diffusion Networks* (GRAD-Net), for unsupervised image retrieval. Inspired by recent developments of graph neural networks, we design two loss functions that directly depict diffusion processes on the image manifolds without any labeled information. The content and strength of the diffusion process is thus fully learn-able, and the features are trained to transform on an ideal manifold with subject to the defined loss in an unsupervised fashion. Benefiting from the generalisability of GNNs, our model can be easily extended to unseen instances. Furthermore, in order to consider global structures in the graphs, we propose to construct an additional bi-part graph as inputs to the proposed GRAD-Net so that we can learn global and local consistent representations of all the images. Last, to alleviate the scalability issue, sub-networks will be effectively sampled at each training iteration. Extensive empirical experiments are conducted on multiple benchmarks to verify the effectiveness of the proposed method.

Specifically, our main contributions are summarized as follows:

- 1) **Unsupervised Representation Learning on Image Manifolds:** GRAD-Net, among the first-in-class deep learning models for unsupervised diffusion process on image retrieval, updates the instance features (i.e., the node attributes on the graphs) us-

ing GRAD-Net in an end-to-end manner instead of following the conventional choice of diffusing rank values or similarities on manifolds. We transform the conventional diffusion from a message-passing process into an optimization process by introducing an efficient diffusion-like operator so that our model can mimic diffusion process with multi-layer neural networks. We show that this approach enriches the features with more semantic information, and the updated features can be used to perform efficient retrieval with a simple nearest neighbor search and **support efficient inductive learning only feasible with our feature learning manner.**

- 2) **Achieving Global and Local Consistency:** Instead of only using sparsified pair-wise graphs (e.g., K-Nearest-Neighbors (KNN) graphs), we design a bi-part graph learned from sparse coding techniques to reflect the global *cluster* information. This additional input together with KNN graphs will reflect both global and local structures with the learned representations. Further, we also design the loss functions to take into consideration of high-order structures from both KNN graphs and Bi-part graphs. Specifically, we introduce two loss functions as objectives describing the ideal manifold properties: the \mathcal{L}_{local} describes the similarity orders along the manifold structure; the \mathcal{L}_{global} defines the distant relations on the manifold. In this way we avoid the human assigned message step in traditional diffusion, and prove that a much more general objective description and following optimization is able to achieve competitive retrieval results.
- 3) **Intrinsic Scalability and High Efficiency:** Unlike traditional diffusion methods which suffer from at least quadratic computational complexity, our model is intrinsically scalable to large database because of near-optimal mini-batch mode training process. Sub-networks can be effectively sampled in the iterative optimization process. The bi-part graph can also reduce the complexity to approximately linear with respect to the number of images in the database. Therefore, our model can achieve fast convergence and high efficiency in both training and querying processes.

2 RELATED WORK

2.1 Diffusion for Unsupervised Image Retrieval

Affinity learning has been a central task for image retrieval. There are a myriad of works focusing on learning a general *metric* (e.g., a Mahalanobis distance) to compute pairwise distances between images [20], [21]. In contrast to conventional metric learning methods, diffusion-based methods have emerged as an alternative promising approach that learns pair-wise similarities on image manifolds. Introduced in [7], diffusion has shown consistent improvements over raw distances/similarities by exploiting intrinsic manifold geometry [22]. Inspired by semi-supervised learning, Graph Transduction (GT) [23] takes the query point as the only labeled data, and propagates the labeled information to unlabeled database in a similar way of label propagation

[24]. Motivated by the observation that a good ranking is usually asymmetrical, Contextual Dissimilarity Measure (CDM) [25] improves Bag-of-Words (BoW) [26] retrieval system by iteratively estimating the pairwise distance in the spirit of Sinkhorn's scaling algorithm.

Further, noticing that diffusion is susceptible to noise edges in the affinity graph, Locally Constrained Diffusion Process (LCDP) [27] stresses that it is crucial to constrain the diffusion process "locally". Along the same line, Tensor Product Graph diffusion (TPG) [28] manages to leverage the high-order information from the tensor product of the affinity graphs but constraining the pathways of message passing to local neighbors only so that the computational complexity does not increase much. A detailed comparison of various diffusion methods has been conducted in a survey [3] by enumerating 72 variants of diffusion process (4 different affinity initialization, 6 different transition matrices and 3 different update schemes). The empirical results suggest that affinity learning on the tensor product graphs with high-order information is more robust in the scope of retrieval. [29] also theoretically explains why this kind of diffusion process is superior by defining a new smoothness criterion among four vertices. And recently [6] enriches the tensor product to a regularization process on graphs and display its potential of retrieval among heterogeneous instances.

2.2 Graph Neural Networks

Recent years have witnessed an increasing interest in applying deep learning algorithms on irregular inputs like graphs. Early work includes recursive neural networks [30] to represent and processing data in graph. Graph Neural Networks (GNNs) were introduced in [31], [32] as a generalization of recursive neural networks that can directly deal with graphs. A typical GNN model consists of an iterative random-walk process in which node states are propagated based on certain probability distribution until equilibrium. This idea was adopted and improved by [33], which propose to use gated recurrent units [34] in the propagation step. However, these recurrent models usually suffer from large computational burden and therefore hard to train and scale to large graphs.

Inspired by the tremendous success of Convolutional Neural Networks (CNNs) in computer vision, [35] introduced the convolution operation in the Fourier domain by computing the eigendecomposition of the graph Laplacian. It was improved then by [36] with a parameterization of the spectral filters with smooth coefficients in order to make them spatially localized. Graph convolutional networks (GCNs) was formally proposed by a landmark work [13] which simplified the previous methods by restricting the filters to operate in a 1-step neighborhood around each node. Since then, various modifications have been proposed to improve upon GCNs. For example, attention mechanism was adopted in [37] to address the issue of high sensitivity to noise in graph edges and instead compute learnable attentions among nodes.

The applications of GNNs in computer vision are growing with notable examples including few-shot image classification [38], [39], semantic segmentation [40], [41], visual

question answering[42], [43]. However, most of these applications of GNNs require extensive amount of labeled data. A recent work [44] reported new GNN layer operations for feature diffusion in a semi-supervised setting. Few literature has focused on image retrieval due to lack of labeled data.

Our work, to our best knowledge, is one of the first attempts to adopt GCN-like algorithms in unsupervised image retrieval. The proposed network requires no labels from humans while extending traditional diffusion models to learn global and local consistent representations for images and enable effective training and query.

3 OUR APPROACH

In this section, we elaborate on the proposed Graph Diffusion Network (Grad-Net) based on the graph convolutional networks [13] and extend the idea of diffusion algorithms [7]. Although our proposed approach can be easily generalized to the retrieval of various types of data, in this paper, we use the diffusion process for image retrieval to illustrate the idea.

3.1 Problem Setup and Notations

For image retrieval tasks, we define a dataset as $\mathcal{X} = \{x_1, x_2, \dots, x_n\} \subset R^d$, where each x_i is a feature vector of an image. In the setting of image retrieval, a set of queries is as well available and can be projected to the same feature space as the datasets' instances. Thus, we denote the queries as $Q = \{q_1, q_2, \dots, q_m\} \subset R^d$, where q_i represents the feature vector of the i -th query image and m is the number of query images. For simplicity, we consider the scenario that the instance (or query) is interpreted as a single vector. And the entire set can be denoted as

$$\bar{\mathcal{X}} = \mathcal{X} \cup Q = \{q_1, \dots, q_m, x_1, \dots, x_n\}. \quad (1)$$

$\bar{\mathcal{X}}_i$ denotes the i -th instance in $\bar{\mathcal{X}}$.

3.2 Diffusion on Graphs

Two main approaches to conduct diffusion on graphs are (i) iterative updating the pair-wise similarities[3], [7] and (ii) solving the closed form directly[5]. However, both approaches are essentially based on the same random walk mechanism proposed by [7].

To perform a random walk on graph G , a transition matrix is defined to describe the probability of walking from one node to another, which is considered to be proportional to the affinity value. Here the degree matrix D is introduced to normalize the affinity matrix and form the transition matrix. The degree matrix $D := \sum_{j=1}^{n+m} a_{ij}$ is a diagonal matrix with each diagonal element corresponding to the row-wise sum of A . Then the transition matrix S is computed as:

$$S = D^{-1/2} A D^{-1/2}. \quad (2)$$

According to the transition matrix S , random walk is then performed on the graph to update a state vector $f^t \in R^{n+m}$ until it converges. For the t -th step of random walk, the process iterates the following step:

$$f^{t+1} = \alpha S f^t + (1 - \alpha) f^0, \alpha \in (0, 1) \quad (3)$$

Specifically, $f^t = [f_q^{tT}, f_d^{tT}]^T$ is composed of both the queries' state $f_q^t \in R^m$ and the datasets' state $f_d^t \in R^n$. The initial state f^0 is set to a binary vector where $f_q^0 = \mathbf{1}$ and $f_d^0 = \mathbf{0}$. Eq.3 can be intuitively interpreted as given a state f^t , it has a probability of α to transit according to S and a probability of $(1-\alpha)$ returning to the initial state. The above process is proved to converge to a closed-form solution[7]:

$$f^* = (1 - \alpha)(I - \alpha S)^{-1} f^0 \quad (4)$$

The final f , derived after given iterations or directly from the close-form solution, is regarded as the similarities between the datasets' instances and the query, which eventually determines the ranking order.

One issue to notice is that Eq.3 does not explicitly consider the high-order information on the manifold. Yang et al.[28] addressed this and introduced a modified diffusion on a tensor product graph, where nodes refer to the instance pairs and thus take into account higher order information naturally. The iteration step in tensor product diffusion is provided as:

$$\hat{A}^{t+1} = S\hat{A}^t S^T + I, \quad (5)$$

The final $\hat{A} \in R^{n \times n}$ after iteration stands for the updated affinity matrix. As reported in [3], the tensor product diffusion achieved the most robust performance in comparison. In this work, we extend the tensor product diffusion into graph convolution operations to exploit the high-order information. The detailed method is introduced in Section 3.4.

3.3 Graph Convolutional Networks

Our proposed Graph Difusion Network is an extention of the the Graph Convolutional Networks(GCN)[13], which provides a one-hop convolution operation on graphs given affinity or adjacent matrices. GCNs contain several hidden layers that take a feature matrix $H^{(l)} \in R^{n \times d_l}$ as the input of the l -th layer and output a feature matrix $H^{(l+1)} \in R^{n \times d_{l+1}}$ by using a graph convolution operator.

Given an input feature matrix $H^{(0)} \in R^{n \times d_0}$ and the graph affinity or adjacent matrix $A \in R^{n \times n}$, GCN as in [13] conducts the following layer-wise propagation as,

$$H^{(l+1)} = \sigma((I + S)H^{(l)}W^{(l)}), \quad (6)$$

where $l \in \{1, 2, \dots, L\}$ and S denotes the same definition as in Eq. 2. $W^l \in R^{d_l \times d_{l+1}}$ is the trainable weight matrix of the layer. $\sigma()$ denotes an activation function. One of the reasons the layer convolution adopted S rather than A is that as layers accumulated, the absolute value of features can easily get larger (or smaller) if the row wise sum of A is above 1 (or below 1), which can cause numerical instabilities. To further alleviate this issue, it is suggested to use the re-normalization of the $(I + S)$ as following:

$$I + D^{-1/2}AD^{-1/2} \rightarrow \hat{D}^{-1/2}\hat{A}\hat{D}^{-1/2}, \quad (7)$$

3.4 Graph Diffusion Networks (GRAD-Net)

We now present our Grad-Net model, which is illustrated in Fig.2. The model is composed of multiple layers of Graph diffusion modules. These layers pass messages between nodes according to the manifold structure and output

the updated node features. Finally, an affinity prediction module accesses the updated features and computes estimated affinities. Several unsupervised loss functions (to be introduced in Section 3.5), which describe the similarities among learned features both globally and locally, are used to regularize the affinity estimation and thus train the model in an end-to-end manner. Apart from the local manifold structure information, a sparse coding feature vector Z is also passed to the Graph Diffusion layer to provide global structure information. The details of the proposed model are as following:

3.4.1 Graph Constructions

In this section, we discuss how to construct graphs as inputs to the proposed networks. To encode both local and global structures from the image manifolds, we design two types of graphs: local sparsified graph and global bi-part graph.

Local Sparsified Graph: To construct the graphs of locality, we follow the mutual K-NN method in [5]. The method computes the K nearest neighbors of every instances and constructs an edge if two nodes are the neighbors of each other. Thus the affinity matrix $A = [a_{ij}] \in R^{N \times N}$, $N = n + m$ is defined as

$$a_{ij} = \begin{cases} s(\bar{\mathcal{X}}_i, \bar{\mathcal{X}}_j), & \bar{\mathcal{X}}_i \in NN_k(\bar{\mathcal{X}}_j), \bar{\mathcal{X}}_j \in NN_k(\bar{\mathcal{X}}_i) \\ 0, & \text{otherwise} \end{cases}, \quad (8)$$

where a_{ij} is an element in A and $i, j \in \{1, 2, \dots, n + m\}$. $s : R^d \times R^d \rightarrow R$ is a predefined similarity metric, typically could be either cosine or euclidean similarity. The chosen s in Eq.8 allows A to be a sparse matrix when K is small, which makes large graph diffusion feasible. So far, the dataset is interpreted as a weighted graph $G_l = (V_l, E_l)$, consisting of $n + m$ nodes $v_i \in V_l$, and the edges $e_{ij} \in E_l$ connect those node pairs which have a non zero value of affinity defined in A . The edge weight is initialised as a_{ij} . Diffusion processes then propagate the affinity values through the entire graph, based on the defined edge weights.

Global Bi-Part Graph by Sparse Coding: To encode the overall cluster information, we adopt a similar idea in [45] in which anchor points are sampled as an estimation of the overall data distribution. We first apply simple clustering algorithm (e.g., K-means) to select B anchor points. In the case of K-means, we can simply use the obtained B centers as the anchor points and denote the feature matrix of these anchor points as $U \in R^{B \times d}$. Then we construct a bi-part graph $G_g = \{V_g, E_g\}$ in which V_g is the union of both original images and the selected anchor points (i.e., $\|V_g\| = N + B$), and E_g denotes all the edges between original images and anchor points (i.e., $E_g \in R^{N \times B}$). We use $Z \in R^{N \times B}$ to represent all the weights on the edge set E_g . Here, we adopt the sparse coding techniques to construct Z . For each image feature $\{\mathbf{x}_i, i = 1, \dots, N\}$, we aim to fully reconstruct it with only s neighboring anchor points. Formally, we learn the weights over edges that connect from x_i to the top c anchor points $\mathbf{z}_i \in R^B$ as follows:

$$\begin{aligned} \min_{\mathbf{z}_i} & \|\mathbf{x}_i - U\mathbf{z}_i\|_2^2 \\ \text{s.t.}, & \ell^T \mathbf{z}_i = 1, \mathbf{z}_i \geq 0, |\mathbf{z}_i| = c \end{aligned} \quad (9)$$

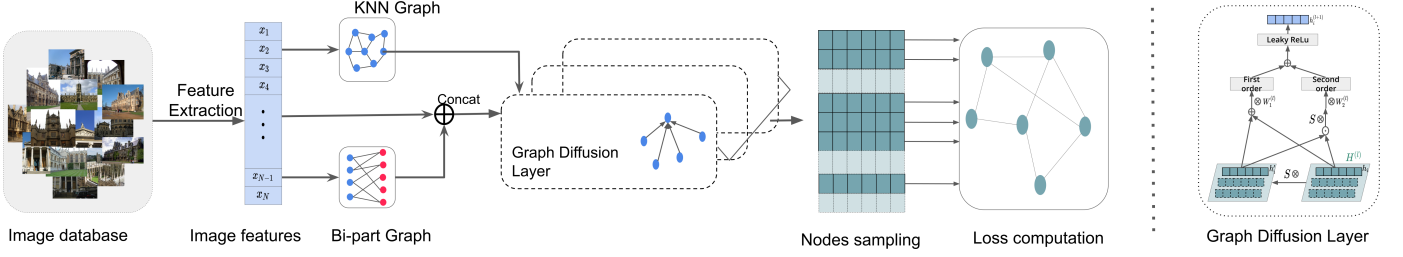


Fig. 2. The pipeline of the proposed Graph Diffusion Network. Given image instances in database, feature extractors firstly extract the feature vectors. The local sparsified (KNN) graph and Bi-part graph are both generated from the features. The GRAD-Net model, containing several graph diffusion layers, then updates the features. Objectives are computed on samples of the output features and in turn train the parameters in the network.

The optimization problem above is a typical sparse coding problem. We directly use the same technique to solve this optimization as [46]. In this way, we can obtain a global bi-part graph with edge weights $Z \in \mathcal{R}^{N \times B}$.

3.4.2 Graph Diffusion Layers.

The constructed graphs $G = \{G_l, G_g\}$ described above serve as the inputs to the Graph diffusion layers. For the purpose of illustration, we consider a general notation for inputs to the graph diffusion layers as follows: the input graph G consists of an affinity matrix $A \in \mathcal{R}^{N \times N}$ and instance features $\bar{\mathcal{X}}$ as in Eq. 1. Here we denote the first layer's input feature matrix $H^{(0)} \in \mathcal{R}^{N \times d}$ as:

$$H^{(0)} = [\bar{\mathcal{X}}_1, \bar{\mathcal{X}}_2, \dots, \bar{\mathcal{X}}_N]^T \quad (10)$$

The Graph Diffusion layer is a variant of graph neural network following the form f_d :

$$H^{(l+1)} = f_d(H^{(l)}, A; W^{(l)}), \quad (11)$$

where $W^{(l)}$ is the trainable parameters of the layer.

To process the graph data and diffuse information among features, we first inherit the idea of the random walk process from conventional diffusion and introduce two operations: first-order operator f_1 and second-order operator f_2 . The total layer function f_d is the combination of both operators.

The first-order operator is a function which generates an updating message for a node u based on its first-order neighbor node i , and thus is defined in its general form as (as a vector operation):

$$m_{u \leftarrow i} = f_1(h_i, p_{u \leftarrow i}), \quad (12)$$

where h_i denotes the layer's feature vector for node i , and relation $p_{u \leftarrow i}$ controls the scale of this message. It can be noticed that, in the conventional diffusion as in Section 3.2, the transition operation Sf^t in Eq.3 serves as the first-order operator. Naturally, we employ this operator in the proposed Graph Diffusion layer and add trainable parameters W . For the l -th layer, the first order function f_1 in the matrix form is

$$m_{u \leftarrow i} = f_1^l = SH^{(l)}W_1^{(l)}. \quad (13)$$

Clearly, this function is consistent to the inner part of the original Graph Convolutional Network in Eq.6.

The second-order operator is defined as a function when updating the feature of a node u which takes in the information of its neighbor's neighbor j . Its general form (as a vector operation) is:

$$m_{u \leftarrow \leftarrow j} = f_2(h_j, p_{u \leftarrow \leftarrow j}), \quad (14)$$

where h_j denotes the layer's feature vector for node j , and relation $p_{u \leftarrow \leftarrow j}$ controls the scale of this message. The double arrow $\leftarrow \leftarrow$ here denotes the fact that j is indirectly connected to u . The difficulty here lies on the design of $p_{u \leftarrow \leftarrow j}$, since node j and i is not directly connected, there is no simple affinity value (as in the case of the first order operation) describing the relation between the two nodes. Nevertheless, in the conventional diffusion, Eq.5 from the work of tensor product [28] provides a solution. As mentioned previously, the partial operation $S\hat{A}^tS^T$ collects the second order information. This can be interpreted as a two-step propagation, where each step transits on the manifold by applying S^T or S and thus pass message to the second order neighbor eventually. Additionally, this operation in Eq.5 displayed superiority regarding both performance and robustness as reported in [3], [28].

To adopt a similar operation but compatible and feasible with end-to-end training, we introduce an approximate function in matrix form as:

$$f_2^l = S(SH^{(l)} \odot H^{(l)})W_2^{(l)}, \quad (15)$$

where \odot denotes the element-wise product, and W_2 is the trainable parameters. The function can also be interpreted as two-step hops, from a group of nodes j to bridging nodes i and then from i to the destination nodes u . To be specific, notice the inner $SH^{(l)}$ resembles the Eq.13 and thus can be viewed as a hop (one step of message passing) on the manifold, namely an $m_{i \leftarrow j}$. Then $m_{i \leftarrow j} \odot H^{(l)}$ serves like an affinity weighting on bridging nodes i 's features, the $H^{(l)}$ here. And finally the whole $S(m_{i \leftarrow j} \odot H^{(l)})W_2^{(l)}$, as another $m_{u \leftarrow i}$, achieves the second hop. This improves the representation ability of Graph Diffusion layer, and achieves performance and robustness gain as well as the tensor product diffusion operation (Eq.5)[28].

Overall, the Graph Diffusion layer performs the propagation as

$$\begin{aligned} H^{(l+1)} &= \sigma(m_{u \leftarrow i} + m_{u \leftarrow \leftarrow j}) \\ &= \sigma((I + S)H^{(l)}W_1^{(l)} + S(SH^{(l)} \odot H^{(l)})W_2^{(l)}), \end{aligned} \quad (16)$$

where σ represents an activation function and is set to LeakyRelu[47] in this work. $H^{(l)} \in R^{n \times d_l}$, $H^{(l+1)} \in R^{n \times d_{l+1}}$ are the layer's input and output features, and $W_1^{(l)}, W_2^{(l)} \in R^{d_l \times d_{l+1}}$ are the trainable parameters, where d_l denotes the dimensions of the features in l -th layer. Note that we also add the I matrix to the first order operation as in Eq.6 in order to introduce the self loop propagation. A group of Graph Diffusion layers are piled sequentially and eventually the network outputs $H^{(L)}$ as the features of nodes. To represent the updated features H after diffusion, one can either use the $H^{(L)}$, or concatenate multiple layers' outputs as

$$H = H^{(0)} \| H^{(1)} \| \dots \| H^{(L)}, \quad (17)$$

where $\|$ is the concatenation along the feature dimension.

Relation to Conventional Diffusion. Comparing Eq.3 to Eq.6, GCN[13] can be regarded as a generalized form of first order diffusion. Additionally, comparing Eq.3 and Eq.5 to Eq.16, our GRAD-Net can be regarded as a generalized form of combined first and second order diffusion (we address Eq.5 as second-order diffusion). Here generalization means that it not only limited to perform propagation on affinity values as conventionally, but also on feature vectors; Also, it supports parameter learning via gradient back propagation. These analogy provides an intuitive explanation on how GRAD-Net diffuses dependency among features as in the random walk process for conventional diffusion.

Affinity Prediction. Pairwise affinity or similarity values can be driven from the updated features $H \in R^{N \times D}$ (Eq.17). Here, we use cosine similarity in all the experiments. Thus, given the node i feature, the i -th row in H , $h_i \in R^D$ and node j feature $h_j \in R^D$, the similarity s_{ij} is

$$s_{ij} = \text{cosine similarity}(h_i, h_j) = \frac{h_i \cdot h_j}{\|h_i\| \|h_j\|}, \quad (18)$$

3.5 Loss Functions for Global and Local Consistence

Loss functions are crucial for training the Grad-Net model. With effective objectives, the features learned can resemble an ideal manifold for image retrieval. Therefore, given the criteria of ideal manifolds, a proper loss function shall regularize the parameters to gradually satisfy the manifold criteria. In this work, we found two effective criteria to describe the feature manifold: *global order* and *local smoothness*, which are capable of training the Grad-Net model to achieve competitive retrieval results. The rest of this section illustrates the details of the two criteria and respectively loss implementations.

Local smoothness refers to the fact that on the given graph $G = (V, E)$ described by affinity matrix A , the similarities of the learned instance features should roughly resemble the low-dimension manifold structure of G in a way that if two nodes are topologically closer in G , the similarity of their features should be higher. To implement this regularization in the objective function, we introduce a pairwise BPR loss following the fashion in[48]:

$$\mathcal{L}_{local} = \sum_{(i,j,u) \in \mathcal{O}_l} -\ln \sigma(s_{ij} - s_{iu}), \quad (19)$$

where $\mathcal{O}_l = \{(i, j, u) | j \in \mathcal{N}_i, u \notin \mathcal{N}_i\}$ denotes the double pair training sample. s_{ij} is the similarity between the

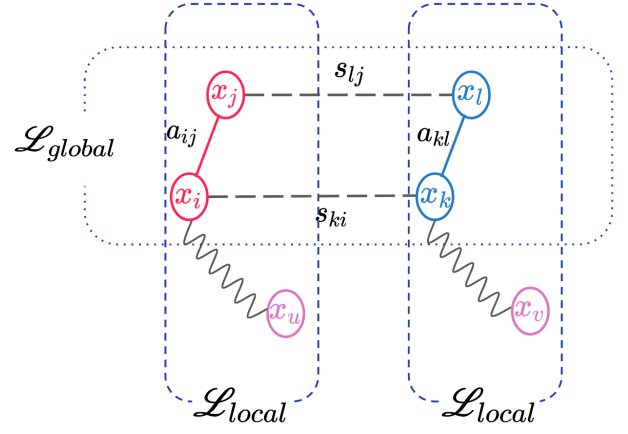


Fig. 3. Loss Interpretation: the x_i and x_j are neighbors, while x_u is far away from x_i on the graph. Similar conditions on x_k, x_l, x_v . Details are described in Section 3.5

features of instances i, j . \mathcal{N}_i refers to the close neighbors of i in the Graph G . The local smoothness loss in Eq.19 can be interpreted that the margin of similarities between a closer node pair and a far-away pair should be large. It is worth noting that the loss is encouraging larger similarities for the nodes in an local neighborhood \mathcal{N}_i . This property is consistent with the empirical finding of [3], [27] that the diffusion process should perform locally on the manifold.

Note that the \mathcal{N}_i can be defined in various forms. Here we define \mathcal{N}_i as the ones sharing direct edge connections with i in Graph G , which yields the best empirical results in Section 4.

Global Order is inspired from the idea in [6], [28] that a cluster of nodes on the manifold should have similar pairwise affinity values across the different pairs within the cluster. [28] introduced tensor product diffusion to inspect a cluster of four nodes simultaneously and thus leverage the higher-order information. Afterwards, [29] provided a regularization form to describe this smoothness. To incorporate this regularization into a loss function suitable for neural networks training, we introduce the following local smoothness loss:

$$\mathcal{L}_{global} = \sum_{(i,j,k,l) \in \mathcal{O}_g} \ln(1 + a_{ij} a_{kl} s_{ki} s_{li} (s_{ki} - s_{lj})^2), \quad (20)$$

where $g = \{(i, j, k, l) | j \in \mathcal{N}_i, j \in \mathcal{N}_k\}$, a_{ij} denotes the original affinity value in the manifold affinity matrix A . The $Loss_{ls}$ can be interpreted as when two pairs of nodes (i, j) and (k, l) close, the similarity across pairs either s_{ki} or s_{lj} should be around the same value.

The final loss is the combination of the two partial loss functions:

$$\mathcal{L} = \mathcal{L}_{local} + \alpha \mathcal{L}_{global} + \lambda \|\Theta\|_2^2, \quad (21)$$

where Θ denotes the model parameters and the $\|\Theta\|_2^2$ is the L2 regularizer on all trainable parameters. $\alpha \in R^+$ and $\lambda \in R^+$ control the proportions of different parts in the final loss.

3.6 Inductive Learning on Unseen Instances

In the existing literature, a query q is by default considered to be contained in the dataset, while this setting is not met

in a lot of real-life scenarios where query is only accessible in production stage after deployment. Conventional Diffusion often hurts from its computation burden and thus lacks the feasibility of processing queries in real time. One representative approach to overcome this difficulty is Query Expansion[49], where given a new query q , its top nearest neighbors x in the database help to estimate similarities to q based on the weighted average of the similarities to x . We follow this idea and derive a fast query expansion approach compatible with our feature learning fashion, the query feature expansion (QFE): After learning a GRAD-Net and recording the output features on a given dataset \mathcal{X} , given a new query q , QFE first find its K nearest neighbors x in the datasets, and then update the feature of q based on its neighbors' features:

$$h_q = \sum_{x \in \mathcal{N}_q} s_{qx} h_x, \quad (22)$$

where h_i denotes the GRAD-Net output feature of node i . So far, h_q is a reasonable approximation feature for q and can be used to retrieval instances via similarity search and rank with all the GRAD-Net output features of \mathcal{X} . Results of the approach is described in 5.3.

3.7 Implementation Details

Here we address several considerations during the implementation and introduce the default configurations for the GRAD-Net model. For all the model variants later in Section 4 and 5, we only clarify the specific changes from this default settings.

Firstly, both the previously mentioned global and local loss functions are descriptors on pair-wise similarities. The global order loss Eq.19 works on triplet features (u, i, j) , while the local smoothness loss Eq.20 works on quadruplet features (i, j, k, l) . Considering this, we provide a compact solution to implement the training process: for each time the model computes forward, a combination of 6 instances is selected to compute the total loss Eq.21 as shown in Fig.3, where the global loss part $Loss_{go}$ are calculated twice from the two triplets (i, j, u) and (k, l, v) , and the local loss part $Loss_{ls}$ are calculated once from the quadruplet (i, j, k, l) . In total, the actual loss function in training is

$$\begin{aligned} \mathcal{L}(i, j, k, l, u, v) \\ = \frac{1}{N_{batch}} \sum_{batch} (\mathcal{L}_{global}(i, j, u) + \mathcal{L}_{global}(k, l, v)) \\ + \alpha \mathcal{L}_{local}(i, j, k, l) + \lambda \|\Theta\|_2^2, \end{aligned} \quad (23)$$

where N_{batch} stands for the number of sextets in a mini batch. Moreover, the training examples in all our experiments are sampled as following: i, k are generated independently from uniform distribution, then j, l are selected randomly from i 's and k 's first-order neighbors respectively, and finally u, v from non-neighbor nodes.

Since the training stage samples sextet instances in the above manner, it is worth noting that there is no concept of the conventional epoch here in our implementation, because the whole possible sextet combinations can reach the degree of $1000^6 = 10^{18}$ even for a dataset of 1k instances. So, to avoid ambiguity, the epoch term we use in this work refers

to the period of training N sextets, where N is the number of instances in a dataset. It is also noticed in our experiments that for datasets with considerable numbers of instances (for example, 5k or 6k), decent performances are obtained within only several epochs, which proves the efficiency of both the model and the training strategy.

The second consideration is to leverage the sparsity of mutual KNN connections and alleviate the computation burden on large datasets. Notice that during the gradient backprop stage for a sextet loss (Eq.23), only the computation paths of nodes which contribute to computing at least one of the sextet (i, j, k, l, u, v) during the forward process will have valid gradients. Therefore, we implement a similar BFS search, as in [50], starting from a batch of sextets ($N_{batch} \times 6$ nodes) to find N'_{batch} relevant nodes. Then the model only processes N'_{batch} of nodes. This acceleration approach has remarkable effect when training large datasets, over 20 times speed up during the training of Oxford105k dataset.

The default configurations for the GRAD-Net are as follows: we set the number of neighbors K in mutual KNN search to 15, and construct the initial affinity matrix with cosines similarity value. We use Adam[51] to optimize the parameters, and set $\alpha = 1e5$ and $\lambda = 1e - 5$ in the loss function Eq.21. A model of three Graph Diffusion layers is constructed with the layers' feature dimensions set to 1024, 256, and 128 respectively. A L2 normalization followed by dropout[52] with a probability of 0.3 is applied to every layer's feature vector output. Mini batch training is performed with the number of sextets in a batch set to 64. All experiments are running on one Nvidia Quadro RTX 5000 GPU. For most variants, it takes from 1-10 seconds to complete one epoch of training.

4 EXPERIMENT

To evaluate the effectiveness of the proposed approach, we conduct experiments on a toy task and four popular benchmark datasets, including various data formats - face in Section 4.2, and natural images in Sections 4.3, 4.4. Table 1 shows the type and statistics of these datasets. All the implementation settings follow the descriptions in Section 3.7.

TABLE 1
Summary of dataset statistics

Dataset	Type	Classes	Instances	Feature Dimensions
ORL	Face	40	400	10304
Oxford5k	Image	11	5062	512 or 2048
Oxford105k	Image	11	105K	512 or 2048
Paris6k	Image	11	6392	2048

4.1 Toy example

We first generate a set of points which construct the word *PAMI* to demonstrate that GRAD-Net can well capture the geometric manifold. As shown in Fig. 4a, each letter contains one query point (marked as a star), and their k -nearest neighbors are shown in green, yellow, blue and purple respectively. Take the query point in letter *M* for example.

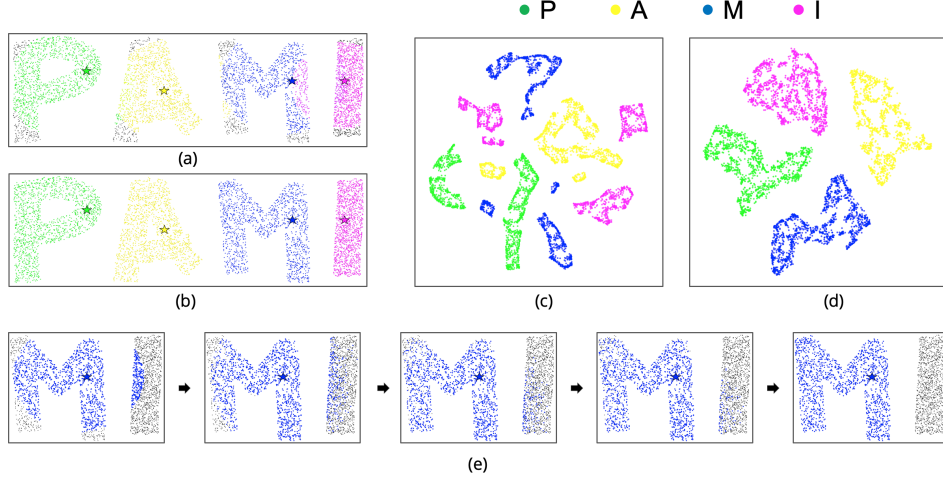


Fig. 4. Synthetic toy dataset results. (a) retrieval results based on euclidean distance; (b) retrieval results after diffusion; (c) t-SNE visualization of the original features; (d) t-SNE visualization of the features after diffusion; (e) intermediate results at different iterations.

Since some points in letter *I* are closer to the points at the corner of *M* in the Euclidean Space, some points are wrongly colored. We take the point coordinates as features and input them to our GRAD-Net. When the diffusion process finishes, all the points are colored correctly (Fig. 4b). The intermediate results at different iterations are shown in Fig. 4e.

We also use a popular visualization method called t-SNE [53] to compare the difference between the original features and the updated features by our model. Fig. 4c and 4d demonstrate that GRAD-Net can make the features more separable after the diffusion process.

4.2 ORL

ORL dataset [54] is a face image dataset that contains 400 images of size 112×92 . There are 10 different images of each of 40 distinct subjects, varying from illuminations, facial expressions and facial details.

We first vectorize the raw image pixels and then normalize them to 0-mean and 1-variance to represent the image. Retrieval accuracy is measured by the the average recall rate at a window size K for each query, also known as the bullseye score. For this dataset, we set $K = 15$ and the baseline bullseye score is 62.35%.

Table 2 reports the performance of various approaches on this dataset. And our GRAD-Net outperforms the state-of-the-art approach by a large margin.

4.3 Oxford5k and Paris6k Dataset

Besides the toy example and comparisons on face dataset presented above, we also examine the proposed GRAD-Net on retrieval tasks with real natural images in this section. Firstly, we adopt the widely-used Oxford5k and Paris6k datasets [56] and use the preprocessing in [5].

Experiments on Oxford5k. The dataset consists of 5062 pictures of 11 different Oxford buildings collected from Flickr and uses 55 query images as ground truth for evaluation. For fair comparison, we employed the features provided in [5] to perform the experiments. In particular, the

image features are provided in two streams: one stream (512 dimension) derived from a VGG net which is fine-tuned for image retrieval [10], while the other stream (2048 dimension) derived from a fine-tuned ResNet101 [57]. Given one instance, [5] extracts one global feature vector and multiple regional feature vectors. In this work, we only consider the scenario where an instance is represented by one feature vector. Therefore, the results in later sections are only compared to models using a single input feature for each instance.

To implement the GRAD-Net for this dataset, we first set the similarity metric to $1/(1 + \text{Euclidean Distance})$, compute an initial dense affinity matrix, and then compare the number of nearest neighbor k as in Eq.8 (details in 5.1) by setting $k = 15$. After searching, we keep all the edges in the mutual KNN graph and set the rest edge weights to zero. So far the input sparse affinity matrix is obtained, where non-zero values represent affinity strength of edges. Another binarised affinity matrix is also tested and demonstrates competitive performance. To compute the sparse features Z , we set the dimension limit to 100 and apply two rounds of *online FSM*. The concatenation of original feature and Z is input to the GRAD-Net model. The model implementation is as Section 3.7 described, with only some specific configurations, including an initial learning rate set to $3e - 4$ and is reduced to 55% respectively after 24 and 100 epochs. The model is trained for 300 epochs, and the training loss, noticed empirically, reaches a stable near-convergence stage after 200 epochs. Thus we simply keep the final model after the last epoch for evaluation.

We compare GRAD-Net with other approaches in Table 3 to evaluate the results. We use the standard evaluation protocol of mean Average Precision (mAP), which has a maximum value of 100%. For both feature choices, the proposed model can significantly improve the baseline performances and achieve the best mAP on both VGG and ResNet features, 90.1 for VGG features and 95.9 for ResNet features. Both results exceed the former state-of-the-art by large margins. It is also noticeable that only a simple nearest neighbor search based on similarities between sparse vectors Z can

TABLE 2
Performance comparison on ORL.

Methods	Baseline	SD [27]	LCDP [55]	TPG [28]	MR [7]	GDP [3]	RDP [6]	Ours
Bullseye score	62.35	71.67	74.25	73.90	77.58	77.42	79.27	84.14

achieve considerable mAP, for example 87.5 with ResNet features. This displays that our proposed sparse coding method is able to capture global similarity relations and reduce the noise in original dense vectors, such that a decent retrieval result can be derived. Furthermore, the GRAD-Net improves additional 8.4 mAP scores with the input of Z , which performance boost results from the graph diffusion process and illustrate that the GRAD-Net features are able to capture the manifold structure. To show the effectiveness of the model itself with and without Z , comparison of model variants are given in Section 5.1.

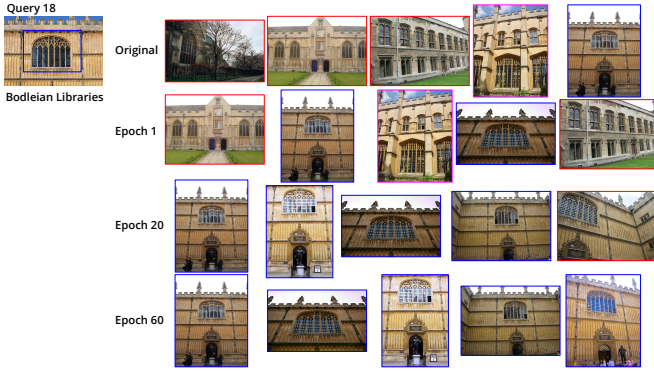


Fig. 5. Retrieval results at different epochs. Query is the image on the top left. Each row on the right contains the top five retrieved images after the corresponding training epoch. Images in the red frames are the incorrect results, while images in the blue frames are the correct ones.

Experiments on Paris6k. The Paris6k dataset is collected in a way very similar to the Oxford5k dataset. It includes 6392 images of 11 Paris buildings from Flickr and uses 55 queries in the ground truth evaluation. We employed the VGG and ResNet features again from [58] and kept the same model configuration as in the previous Oxford5k experiment. Only the K is changed to 60. Results in Table 3 show that the proposed model outperforms the former state of the arts again on both choices of features. Paris

4.4 Oxford105k Dataset

We also validate our GRAD-Net on larger dataset, the Oxford105k dataset, to examine the scalability of our method. The dataset is an extension of the 5k dataset proposed by [5], where another set of 100k random images from Flickr is added as distractor. Due to its size, conventional diffusion methods are typically not capable to run on the whole dataset with in acceptable time. For example, it is reported in [5] that a full diffusion for one query takes 13.9s on with a 12-core CPU. Therefore, former works like [5], [6] have to perform truncation on the 105k instances based on the initial similarity values. For a given query, a truncated graph in [6] is clipped with top 500 nearest nodes and all the diffusion process is running later on the graph.

In this work, the proposed GRAD-Net is capable to train and predict on the whole 105k dataset within feasible time consumption. Due to the relevant node search proposed in Section 3.7, the computation is largely reduced. To accelerate the training, we adopt the aforementioned truncation approach and modify it as following: 1. we select the top-500 nearest instances for each query and union them together to form a union graph. The graph contains around 8k nodes using the ResNet features and 10k nodes using the VGG features. 2. The GRAD-Net model is trained on the union graph and the learned feature is then used to retrieval.

As shown in3, the proposed approach achieves outstanding performance (mAP 94.5) on the ResNet version and outperform the former best result on single global feature[59] by 2.7. Using the VGG version, the model also achieves a competitive result. We examine that the union graph generated from VGG features typically throw away more correct instances, this give an intuitive explanation on why the training becomes difficulty.

5 DISCUSSION

5.1 Ablation Study

In this section, we vary the configurations of several important modules or settings in the proposed GRAD-Net . The results verify the effectiveness of corresponding parts and provide intuition for optimal hyper-parameters. For the purpose of illustrating the concepts, we only focus on the Oxford5k dataset and set the "default" model as in Section 4.3, which achieves a mAP score of 95.95.

To take fair comparison among different model variants, we run 6 trails for each variant and examine the records on three evaluation metrics:

- 1) *Epochs mAP92+* refers to the number of epochs that the model takes during training to first reach a mAP of 92. Since 92 is a considerable decent accuracy, we use this number to examine learning efficiency.
- 2) *mAP* is the previously mentioned mean Average Precision score. After recording the 6 mAP scores for 6 trials, the average over trial and the standard deviation are reported here.
- 3) *Diff* refers to the mAP drop compared to the default model (the first row in Table 4).

Loss functions. Two different losses have been proposed previously, including the order-preserving loss and the local smoothness loss. Different variants of models here test the validity of each one working alone and the combination. Ablation of any loss stated before shows noticeable performance drop and the most considerable influence is the one of \mathcal{L}_{local} loss. Without the local loss, the model only can reach 90.16 average precision and also shows a slight increase of instability in training. The global loss \mathcal{L}_{global}

TABLE 3
Performance comparison on Oxford5k, Oxford105k, and Paris6k.

Method	Feature	Oxford5k	Oxford105k	Paris6k
k-NN search	VGG	79.5	72.1	84.5
k-NN + AQE[49]		85.4	79.7	88.4
Reginal Diffusion[5]		85.7	82.7	94.1
Eff Diffusion[59]		89.7	86.8	94.7
GDN(Ours)		90.1	84.6	94.8
k-NN search	ResNet	83.6	80.8	93.8
k-NN + AQE[49]		89.6	88.3	95.3
Reginal Diffusion[5]		87.1	87.4	96.5
Eff Diffusion[59]		92.6	91.8	97.1
GDN(Ours)		95.9	94.5	97.3

shows less influence on the retrieval precision, but its absence increase the deviation to 0.41. It is worth to mention that the ablation test only give us intuitions on the way how the loss interect with the training process, but it does not directly judge the exact amount of the loss function’s effect since all the modules and losses can work in compensation. **Sparse Coding.** The sparse encoding vector Z is another important part in the Grad-net. As default, Z is an 100 dimensional vector append to the input CNN features. Here we test on three variants related to Z , respectively (1) project Z to a dense vector \bar{X} , (2) No sparse vector Z and (3) only using Z but no raw feature. We found that adding Z is useful to generate precision improvement, while the raw feature is still essential for the retrieval. **Graph Structure.** Different layer settings are tested, results show that the model is relatively robust to the layer size and number of layers at least on this dataset. The interesting comparison is that we replace our Graph Diffusion layer, which includes a second order operator, with the vanilla GCN[13] network and the results show a considerable 0.96 mAP drop. This empirically shows the proposed operator’s effectiveness. **Manifold Structure.** Tests on manifold structures clearly display that the manifold determined by the K number in mutual NN search is crucial for the learning result. K is most prefered around. The following similarity metric variants also may vary the manifold structure. However, the model shows relatively robustness to this hyper-parameter.

5.2 Feature Learning

The most noticeable difference between our method and the conventional diffusion is that here GRAD-Net performs feature learning and outputs updated features rather than merely similarity values. The training process can be summarized and interpreted as learning to share information among instances to a degree that the updated features can explicitly become similar to those that locate very close with them on the low-dimensional manifold. Therefore, We intuitively hope the features learned can display high level characteristics that learned from the training process, including better representation of the semantic information and closer clustering for instances with similar semantic information.

Thus, we test these characteristics by comparing the original features and learned features with clustering methods

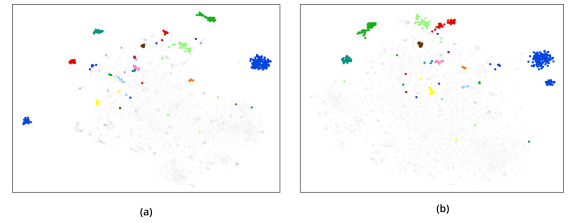


Fig. 6. The feature learning results. (a) t-SNE visualization of the original features; (b) t-SNE visualization of the learned features.

and visualizing on lower dimensions. Fig. 6 is acquired by using tsne on Oxford5k features before and after the model processing. We use the ground truth label to select and visualize the nodes of classes in different colors. It clearly displays that the features provided by the proposed model can form clusters within images of the same category.

5.3 Inductive Learning

To test the model’s generalization ability for new queries, we manually separate 11 queries from the 55 queries of the Oxford5k dataset and leave them out in training. We then retrieve from all the visible part of dataset given this 11 queries using the QFE method described in Section 3.6. The result mAP in the Table. 5 shows the effectiveness of the QFE method. And by applying QFE for the second time, a slightly improvement id gained since the feature can be updated again from the search.

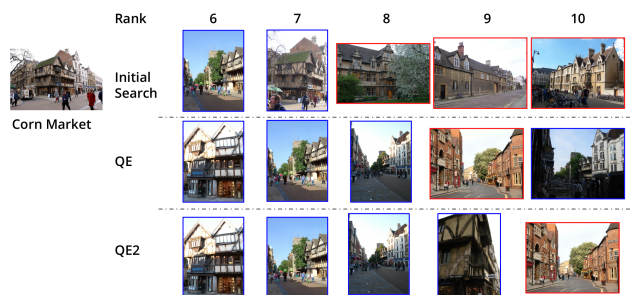


Fig. 7. Query Induction Example. A two stage query induction expansion: the first row represents the initial search in the raw feature space. The second row represents the first QFE search result, and the third row is the second time QFE. It is clear that QFE can improve the retrieval results.

TABLE 4

Interpretation of modules in Grad-net. The content is divided into different groups of experiments. The bold entries are those receives the most significant influences in the certain group of experiments.

Category	Variants	epochs	mAP92+	mAP	Diff
-	default	9	95.95±0.26	-	-
loss (default Eq.21)	No \mathcal{L}_{local}	-	90.16±0.39	2.54	
	No \mathcal{L}_{global}	11	95.59± 0.41	0.36	
	No $\ \Theta\ _2^2$	8	95.64±0.39	0.31	
coding (default - Z & raw feature)	$\bar{X} = WZ$	10	95.24±0.84	0.75	
	Only raw feature	12	95.56±0.24	0.39	
	Only Z	-	89.51±0.53	6.44	
model structure (default-1024, 256, 128)	Layers-1024,256,128,128	9	95.28±0.35	0.67	
	Layers-1024,256	9	95.55±0.39	0.40	
	Layers-512,128,64	15	95.39± 0.64	0.56	
	GCN[13] no 2nd order	8	94.99±0.52	0.96	
manifold structure (default K=15)	K=8	30	93.07±0.54	2.88	
	K=20	12	95.21±0.48	0.74	
	K=25	10	94.03±0.67	1.92	
	K=32	8	92.68±0.62	3.35	
	K=64	-	90.37±0.47	5.58	
similarity metric (default-Euclidean)	Binary Cosine	9	95.67±0.39	0.28	
	Gaussian Euclidean[28]	30	94.36±0.58	1.59	
	Weighted Cosine	28	94.63±0.64	1.32	
training (default batch=64)	batch=32	10	95.37± 0.47	0.58	
	batch=128	15	95.40±0.27	0.55	
	batch=256	21	94.84±0.30	1.11	
	batch=1024	62	93.69±0.37	2.04	

As shown in Fig. 7, the QFE can project the query's feature approximately to the learned feature space and result in a much accurate rank order.

TABLE 5
Performance comparison on multiple calls

Method	Model	mAP
Query Expansion	Regional Diffusion[5]	89.6
QFE	GDN	96.01
QFE × 2		96.05

6 CONCLUSION

In this paper, we address the problem of unsupervised image retrieval via a novel deep learning based method, GRAD-Net, which adopts graph neural networks on image similarity graphs. In contrast to existing diffusion methods, GRAD-Net enables effective representation learning for images while preserving both local and global geometric properties of image manifolds. Further, it can be trained in an unsupervised end-to-end fashion and easily scalable to large datasets. Extensive empirical results on multiple benchmarks for image retrieval demonstrate the effectiveness of our method.

REFERENCES

- [1] M. R. Ghorab, D. Zhou, A. Oconnor, and V. Wade, "Personalised information retrieval: Survey and classification," *User Modeling and User-Adapted Interaction*, vol. 23, no. 4, pp. 381–443, 2013.
- [2] D. Van Aken, A. Pavlo, G. J. Gordon, and B. Zhang, "Automatic database management system tuning through large-scale machine learning," in *Proceedings of the 2017 ACM International Conference on Management of Data*, ACM, 2017, pp. 1009–1024.
- [3] M. Donoser and H. Bischof, "Diffusion processes for retrieval revisited," in *Proceedings of the IEEE conference on computer vision and pattern recognition*, 2013, pp. 1320–1327.
- [4] F. Bach, "Breaking the curse of dimensionality with convex neural networks," *The Journal of Machine Learning Research*, vol. 18, no. 1, pp. 629–681, 2017.
- [5] A. Iscen, G. Tolias, Y. Avrithis, T. Furon, and O. Chum, "Efficient diffusion on region manifolds: Recovering small objects with compact cnn representations," in *Proceedings of the IEEE Conference on Computer Vision and Pattern Recognition*, 2017, pp. 2077–2086.
- [6] S. Bai, X. Bai, Q. Tian, and L. J. Latecki, "Regularized diffusion process on bidirectional context for object retrieval," *IEEE transactions on pattern analysis and machine intelligence*, vol. 41, no. 5, pp. 1213–1226, 2018.
- [7] D. Zhou, J. Weston, A. Gretton, O. Bousquet, and B. Schölkopf, "Ranking on data manifolds," in *Advances in neural information processing systems*, 2004, pp. 169–176.
- [8] A. Babenko, A. Slesarev, A. Chigorin, and V. Lempitsky, "Neural codes for image retrieval," in *European conference on computer vision*, Springer, 2014, pp. 584–599.
- [9] A. Gordo, J. Almazn, J. Revaud, and D. Larlus, "Deep image retrieval: Learning global representations for

- image search," in *European conference on computer vision*, Springer, 2016, pp. 241–257.
- [10] F. Radenovi, G. Tolias, and O. Chum, "Cnn image retrieval learns from bow: Unsupervised fine-tuning with hard examples," in *European conference on computer vision*, Springer, 2016, pp. 3–20.
- [11] A. S. Razavian, J. Sullivan, S. Carlsson, and A. Maki, "Visual instance retrieval with deep convolutional networks," *IEEE Transactions on Media Technology and Applications*, vol. 4, no. 3, pp. 251–258, 2016.
- [12] J. Deng, W. Dong, R. Socher, L.-J. Li, K. Li, and L. Fei-Fei, "Imagenet: A large-scale hierarchical image database," in *2009 IEEE conference on computer vision and pattern recognition*, Ieee, 2009, pp. 248–255.
- [13] T. N. Kipf and M. Welling, "Semi-supervised classification with graph convolutional networks," *ArXiv preprint arXiv:1609.02907*, 2016.
- [14] J. Atwood and D. Towsley, "Diffusion-convolutional neural networks," in *Advances in Neural Information Processing Systems*, 2016, pp. 1993–2001.
- [15] M. Niepert, M. Ahmed, and K. Kutzkov, "Learning convolutional neural networks for graphs," in *International conference on machine learning*, 2016, pp. 2014–2023.
- [16] S. Cao, W. Lu, and Q. Xu, "Deep neural networks for learning graph representations," in *Thirtieth AAAI Conference on Artificial Intelligence*, 2016.
- [17] R. Levie, F. Monti, X. Bresson, and M. M. Bronstein, "Cayleynets: Graph convolutional neural networks with complex rational spectral filters," *IEEE Transactions on Signal Processing*, vol. 67, no. 1, pp. 97–109, 2018.
- [18] X. Wang, X. He, M. Wang, F. Feng, and T.-S. Chua, "Neural graph collaborative filtering," *ArXiv preprint arXiv:1905.08108*, 2019.
- [19] N. Park, A. Kan, X. L. Dong, T. Zhao, and C. Faloutsos, "Estimating node importance in knowledge graphs using graph neural networks," *ArXiv preprint arXiv:1905.08865*, 2019.
- [20] D. P. Vassileios Balntas Edgar Riba and K. Mikolajczyk, "Learning local feature descriptors with triplets and shallow convolutional neural networks," in *Proceedings of the British Machine Vision Conference (BMVC)*, E. R. H. Richard C. Wilson and W. A. P. Smith, Eds., BMVA Press, Sep. 2016, pp. 119.1–119.11, ISBN: 1-901725-59-6. DOI: 10.5244/C.30.119. [Online]. Available: <https://dx.doi.org/10.5244/C.30.119>.
- [21] R. Yu, Z. Dou, S. Bai, Z. Zhang, Y. Xu, and X. Bai, "Hard-aware point-to-set deep metric for person re-identification," in *Proceedings of the European Conference on Computer Vision (ECCV)*, 2018, pp. 188–204.
- [22] D. Zhou, O. Bousquet, T. N. Lal, J. Weston, and B. Schölkopf, "Learning with local and global consistency," in *Advances in neural information processing systems*, 2004, pp. 321–328.
- [23] X. Bai, X. Yang, L. J. Latecki, W. Liu, and Z. Tu, "Learning context-sensitive shape similarity by graph transduction," *IEEE Transactions on Pattern Analysis and Machine Intelligence*, vol. 32, no. 5, pp. 861–874, 2009.
- [24] U. N. Raghavan, R. Albert, and S. Kumara, "Near linear time algorithm to detect community structures in large-scale networks," *Physical review E*, vol. 76, no. 3, p. 036 106, 2007.
- [25] H. Jegou, C. Schmid, H. Harzallah, and J. Verbeek, "Accurate image search using the contextual dissimilarity measure," *IEEE Transactions on Pattern Analysis and Machine Intelligence*, vol. 32, no. 1, pp. 2–11, 2008.
- [26] L. Fei-Fei and P. Perona, "A bayesian hierarchical model for learning natural scene categories," in *2005 IEEE Computer Society Conference on Computer Vision and Pattern Recognition (CVPR'05)*, IEEE, vol. 2, 2005, pp. 524–531.
- [27] B. Wang and Z. Tu, "Affinity learning via self-diffusion for image segmentation and clustering," in *2012 IEEE Conference on Computer Vision and Pattern Recognition*, IEEE, 2012, pp. 2312–2319.
- [28] X. Yang, L. Prasad, and L. J. Latecki, "Affinity learning with diffusion on tensor product graph," *IEEE transactions on pattern analysis and machine intelligence*, vol. 35, no. 1, pp. 28–38, 2012.
- [29] S. Bai, X. Bai, Q. Tian, and L. J. Latecki, "Regularized diffusion process for visual retrieval," in *Thirty-First AAAI Conference on Artificial Intelligence*, 2017.
- [30] P. Frasconi, M. Gori, and A. Sperduti, "A general framework for adaptive processing of data structures," *IEEE transactions on Neural Networks*, vol. 9, no. 5, pp. 768–786, 1998.
- [31] M. Gori, G. Monfardini, and F. Scarselli, "A new model for learning in graph domains," in *Proceedings. 2005 IEEE International Joint Conference on Neural Networks*, 2005., IEEE, vol. 2, 2005, pp. 729–734.
- [32] F. Scarselli, M. Gori, A. C. Tsoi, M. Hagenbuchner, and G. Monfardini, "The graph neural network model," *IEEE Transactions on Neural Networks*, vol. 20, no. 1, pp. 61–80, 2008.
- [33] Y. Li, D. Tarlow, M. Brockschmidt, and R. Zemel, "Gated graph sequence neural networks," *ArXiv preprint arXiv:1511.05493*, 2015.
- [34] K. Cho, B. Van Merriënboer, C. Gulcehre, D. Bahdanau, F. Bougares, H. Schwenk, and Y. Bengio, "Learning phrase representations using rnn encoder-decoder for statistical machine translation," *ArXiv preprint arXiv:1406.1078*, 2014.
- [35] J. Bruna, W. Zaremba, A. Szlam, and Y. LeCun, "Spectral networks and locally connected networks on graphs," *ArXiv preprint arXiv:1312.6203*, 2013.
- [36] M. Henaff, J. Bruna, and Y. LeCun, "Deep convolutional networks on graph-structured data," *ArXiv preprint arXiv:1506.05163*, 2015.
- [37] P. Velickovi, G. Cucurull, A. Casanova, A. Romero, P. Lio, and Y. Bengio, "Graph attention networks," *ArXiv preprint arXiv:1710.10903*, 2017.
- [38] V. Garcia and J. Bruna, "Few-shot learning with graph neural networks," *ArXiv preprint arXiv:1711.04043*, 2017.
- [39] M. Guo, E. Chou, D.-A. Huang, S. Song, S. Yeung, and L. Fei-Fei, "Neural graph matching networks for fewshot 3d action recognition," in *Proceedings of the European Conference on Computer Vision (ECCV)*, 2018, pp. 653–669.

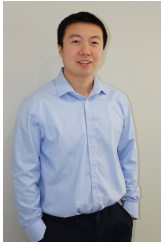
- [40] X. Qi, R. Liao, J. Jia, S. Fidler, and R. Urtasun, "3d graph neural networks for rgbd semantic segmentation," in *Proceedings of the IEEE International Conference on Computer Vision*, 2017, pp. 5199–5208.
- [41] L. Yi, H. Su, X. Guo, and L. J. Guibas, "Syncspecnn: Synchronized spectral cnn for 3d shape segmentation," in *Proceedings of the IEEE Conference on Computer Vision and Pattern Recognition*, 2017, pp. 2282–2290.
- [42] X. Chen, L.-J. Li, L. Fei-Fei, and A. Gupta, "Iterative visual reasoning beyond convolutions," in *Proceedings of the IEEE Conference on Computer Vision and Pattern Recognition*, 2018, pp. 7239–7248.
- [43] M. Narasimhan, S. Lazebnik, and A. Schwing, "Out of the box: Reasoning with graph convolution nets for factual visual question answering," in *Advances in Neural Information Processing Systems*, 2018, pp. 2654–2665.
- [44] B. Jiang, D. Lin, J. Tang, and B. Luo, "Data representation and learning with graph diffusion-embedding networks," in *Proceedings of the IEEE Conference on Computer Vision and Pattern Recognition*, 2019, pp. 10414–10423.
- [45] W. Liu, J. He, and S.-F. Chang, "Large graph construction for scalable semi-supervised learning," in *Proceedings of the 27th international conference on machine learning (ICML-10)*, 2010, pp. 679–686.
- [46] X. Lan, S. Zhang, P. C. Yuen, and R. Chellappa, "Learning common and feature-specific patterns: A novel multiple-sparse-representation-based tracker," *IEEE Transactions on Image Processing*, vol. 27, no. 4, pp. 2022–2037, 2017.
- [47] B. Xu, N. Wang, T. Chen, and M. Li, "Empirical evaluation of rectified activations in convolutional network," *ArXiv preprint arXiv:1505.00853*, 2015.
- [48] S. Rendle, C. Freudenthaler, Z. Gantner, and L. Schmidt-Thieme, "Bpr: Bayesian personalized ranking from implicit feedback," in *Proceedings of the twenty-fifth conference on uncertainty in artificial intelligence*, AUAI Press, 2009, pp. 452–461.
- [49] O. Chum, J. Philbin, J. Sivic, M. Isard, and A. Zisserman, "Total recall: Automatic query expansion with a generative feature model for object retrieval," in *2007 IEEE 11th International Conference on Computer Vision*, IEEE, 2007, pp. 1–8.
- [50] W. Hamilton, Z. Ying, and J. Leskovec, "Inductive representation learning on large graphs," in *Advances in Neural Information Processing Systems*, 2017, pp. 1024–1034.
- [51] D. P. Kingma and J. Ba, "Adam: A method for stochastic optimization," in *3rd International Conference on Learning Representations, ICLR 2015*, 2015. [Online]. Available: <http://arxiv.org/abs/1412.6980>.
- [52] N. Srivastava, G. Hinton, A. Krizhevsky, I. Sutskever, and R. Salakhutdinov, "Dropout: A simple way to prevent neural networks from overfitting," *The journal of machine learning research*, vol. 15, no. 1, pp. 1929–1958, 2014.
- [53] L. v. d. Maaten and G. Hinton, "Visualizing data using t-sne," *Journal of machine learning research*, vol. 9, no. Nov, pp. 2579–2605, 2008.
- [54] F. S. Samaria and A. C. Harter, "Parameterisation of a stochastic model for human face identification," in *Proceedings of 1994 IEEE Workshop on Applications of Computer Vision*, IEEE, 1994, pp. 138–142.
- [55] X. Yang, S. Koknar-Tezel, and L. J. Latecki, "Locally constrained diffusion process on locally densified distance spaces with applications to shape retrieval," in *2009 IEEE Conference on Computer Vision and Pattern Recognition*, IEEE, 2009, pp. 357–364.
- [56] J. Philbin, O. Chum, M. Isard, J. Sivic, and A. Zisserman, "Object retrieval with large vocabularies and fast spatial matching," in *2007 IEEE Conference on Computer Vision and Pattern Recognition*, IEEE, 2007, pp. 1–8.
- [57] A. Gordo, J. Almazan, J. Revaud, and D. Larlus, "End-to-end learning of deep visual representations for image retrieval," *International Journal of Computer Vision*, vol. 124, no. 2, pp. 237–254, 2017.
- [58] J. Philbin, O. Chum, M. Isard, J. Sivic, and A. Zisserman, "Lost in quantization: Improving particular object retrieval in large scale image databases," in *2008 IEEE conference on computer vision and pattern recognition*, IEEE, 2008, pp. 1–8.
- [59] F. Yang, R. Hinami, Y. Matsui, S. Ly, and S. Satoh, "Efficient image retrieval via decoupling diffusion into online and offline processing," in *Proceedings of the AAAI Conference on Artificial Intelligence*, vol. 33, 2019, pp. 9087–9094.



Zhiyong Dou received the B.S. degree electric and electronic engineering from the Huazhong University of Science and Technology, Wuhan, China in 2017, where he is currently pursuing the Ph.D. degree with the School of Electronic Information and Communications. His current research interests include computer vision, computational biology and machine learning.



Haotian Cui received the B.S. degree in Biomedical Engineering from the Tsinghua University, China in 2015. He is currently pursuing the Ph.D. degree at University of Toronto. His current research interests include computer vision, computational biology and machine learning.



Bo Wang is a Scientist at the Peter Munk Cardiac Center of University Health Network, and Assistant Professor in the Dept. of Medical Biophysics at the University of Toronto. Dr. Wang earned a Masters Degree in Computer Science from University of Toronto, Canada in 2012 and a Ph.D. Degree in Computer Science from the Stanford University, USA in 2017. Dr. Wang started his own laboratory in Toronto in 2018. He is also named as one of the CIFAR AI chairs at Vector Institute, Toronto, Canada in 2019. His

current research interests include computer vision, computational biology and machine learning.